Electronic Supplementary Material (ESI) for Journal of Materials Chemistry C.

Supporting Information

Scalable and self-supported $FeNi_3/Mo_2C$ flexible paper for enhanced electromagnetic wave absorption evaluated via coaxial, waveguide and arch methods

Chen Wu[1*], Kai Bi[1] and Mi Yan[1*]

1 School of Materials Science and Engineering, State Key Laboratory of Silicon Materials, Zhejiang University, Hangzhou310027, China

**E-mail: chen_wu@zju.edu.cn;mse_yanmi@zju.edu.cn*

Figure S1 shows the photo images taken from the testing samples for the coaxial, waveguide and arch. The coaxial sample exhibit a ring shape with outer diameter = 7.00 mm, inner diameter = 3.04 mm and thickness = 2.00 mm, while dimensions for the samples prepared for waveguide and arch measurements are 22.86 mm × 10.16 mm × 2.00 mm and 100.00 mm×100.00 mm × 2.00 mm, repectively.

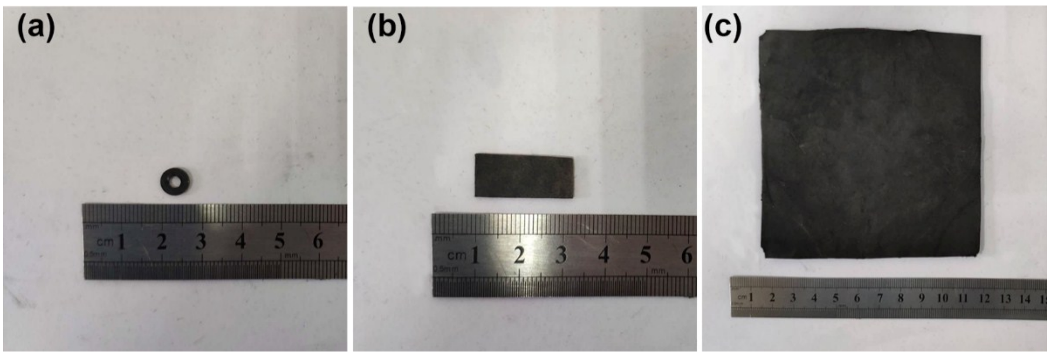

Fig S1 Photo taken from the testing samples prepared for the (a) coaxial, (b) waveguide and (c) arch method

Figure S2 shows the complex permittivity and permeability of the $FeNi_3/Mo_2C$ papers with the $Mo_2C/FeNi_3$ ratio varied between 4:1 and 2:1 compared to those of the Mo_2C alone. The ε' and ε'' decrease after the introduction of the $FeNi_3$ with similar trend observed for the $\tan\delta_e$ (Fig. S2c). The μ' and μ'' gradually increase with raised $FeNi_3$ content (Fig. S2d and S2e), and $\tan\delta_m$ in Fig. S2f exhibit a board resonance peak at around 10.3 GHz..

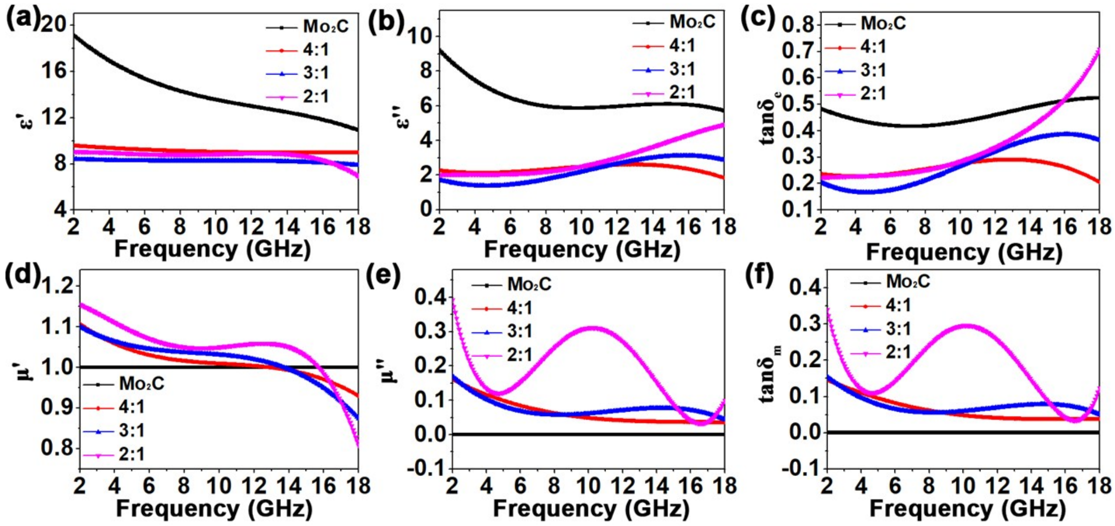

Fig. S2 (a) Real (ε') and (b) imaginary (ε'') part of the permittivity and (c) the corresponding dielectric loss tangent. (d) Real (μ') and (e) imaginary (μ'') permeability and (f) the magnetic loss tangent for the $FeNi_3/Mo_2C$ papers with varied $FeNi_3/Mo_2C$ ratio

Figure S3a-S3d show the Reflection loss (RL) of $FeNi_3/Mo_2C$ papers with different $FeNi_3/Mo_2C$ ratio. The absorbing performance of the Mo_2C paper is the worst with the minimum RL of around -18.30 dB. Increased of $FeNi_3$ ratio gives rise to improved absorbing performance. When $Mo_2C:FeNi_3$ = 3:1, optimized absorption of RL = -51.50 dB and EAB = 5.1 GHz at the thickness of 2.0 mm is obtained as shown in Figure S3c. Further decreasing the $Mo_2C:FeNi_3$ ratio to 2:1 leads to deteriorated absorption of RL = -39.85 dB at the thickness of 3.5 mm.

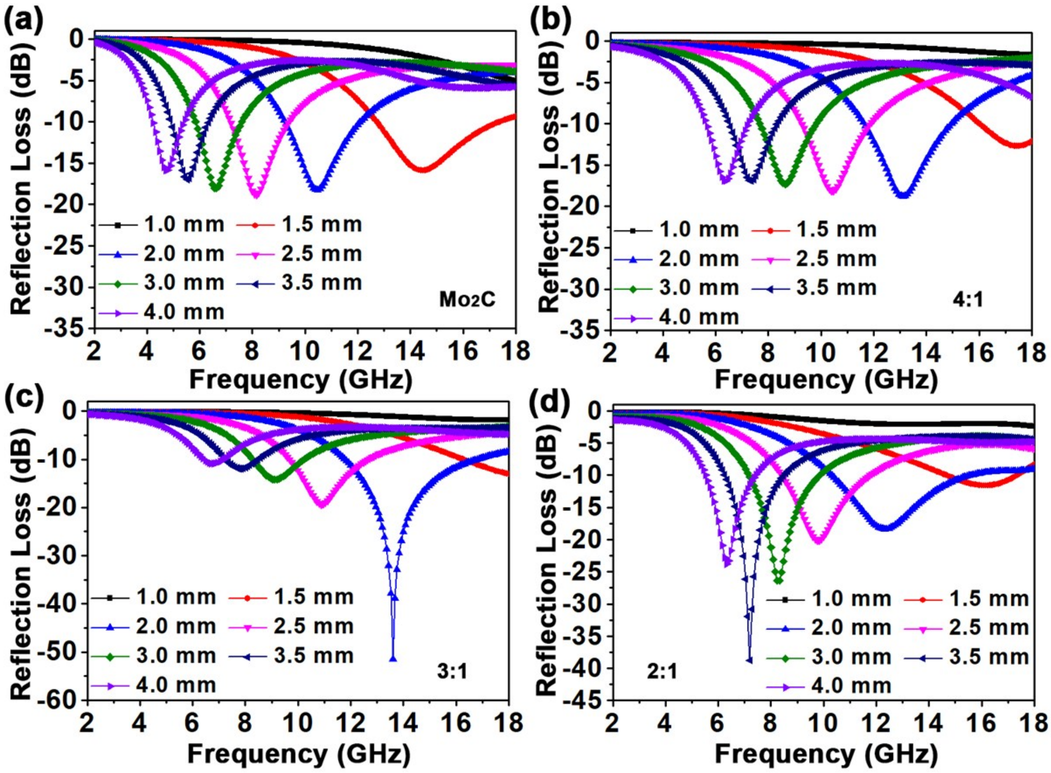

Fig.S3 RL as a function of frequency for the flexible papers containing (a) the Mo_2C and the composites with the $Mo_2C/FeNi_3$ molar ratio of (b) 4:1, (c) 3:1 and (d) 2:1

To understand the reaction process during the co-precipitation of Fe^{2+} and Ni^{2+}, effects of the Fe^{2+} concentration, reaction time and temperature have been investigated. Fig.S4a compares the XRD of the resultants obtained by varying the Fe^{2+} molar concentration from 0% to 10% and 25%with enlarged area indicated by the dashed rectangle shown in Fig.S4b where no Fe-related peak is observed and the (001) peak of $Ni(OH)_2$ shifts from 22.40° to 22.74° and 22.81° with raised Fe concentration, indicating incorporation of the Fe in the $Ni(OH)_2$. Fig.S4c and S4e illustrate the changes of the XRD curves for the resultants obtained with increased reaction time and temperature from 10 min to 120 min and from 40 °C to 80 °C with the corresponding enlargements shown in Fig. S4d and S4f. With the reaction proceeds, the area ratio of $FeNi_3$ increases from 22.6% to 78.7% for increased reaction temperature

(Fig. S4d) and from 41.9 % to 76.3 % with extended reaction time (Fig. S4f), suggesting the transition from the Fe-incoporated $Ni(OH)_2$ into the $FeNi_3$ during the reaction.

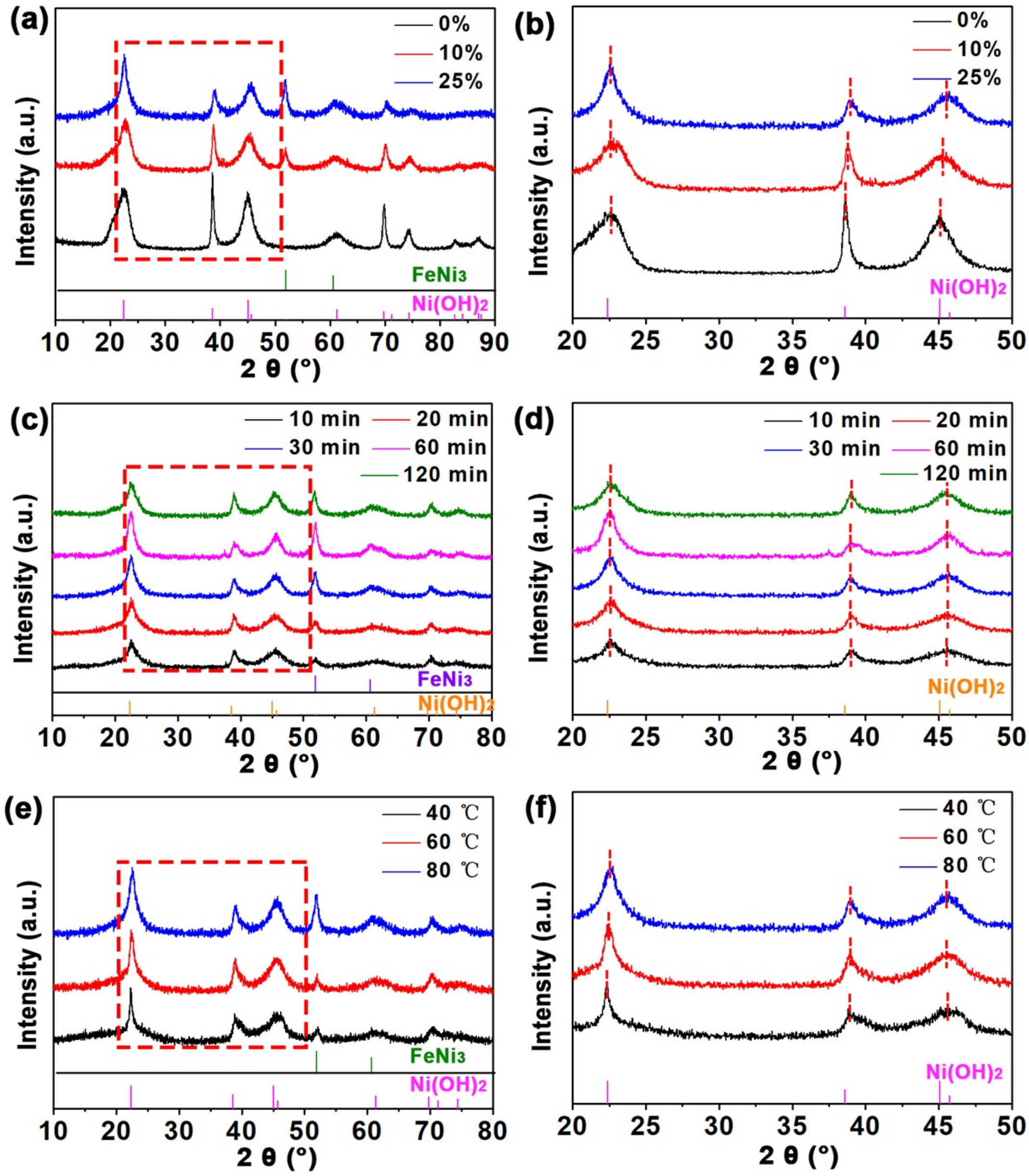

Fig. S4 XRD patterns taken from the resultants from the co-precipitation of Fe^{2+} and Ni^{2+}, showing their evolution with varied Fe^{2+} concentration, reaction timeand temperature.

As shown in Fig. S5, when the content of $FeNi_3/Mo_2C$ in the paper increases from 20 wt%, 30 wt% to

40 wt%, the ε' increases from around 6 to 16, and the ε'' increases from approx 1 to 6 with the $\tan\delta_e$ exhibiting similar trend. For permeability, the raised $FeNi_3/Mo_2C$ content gives rise to slightly increased μ' and μ''. Similar trend is observed for the $\tan\delta_m$ with the appearance of resonance peaks as shown in Figure S5f.

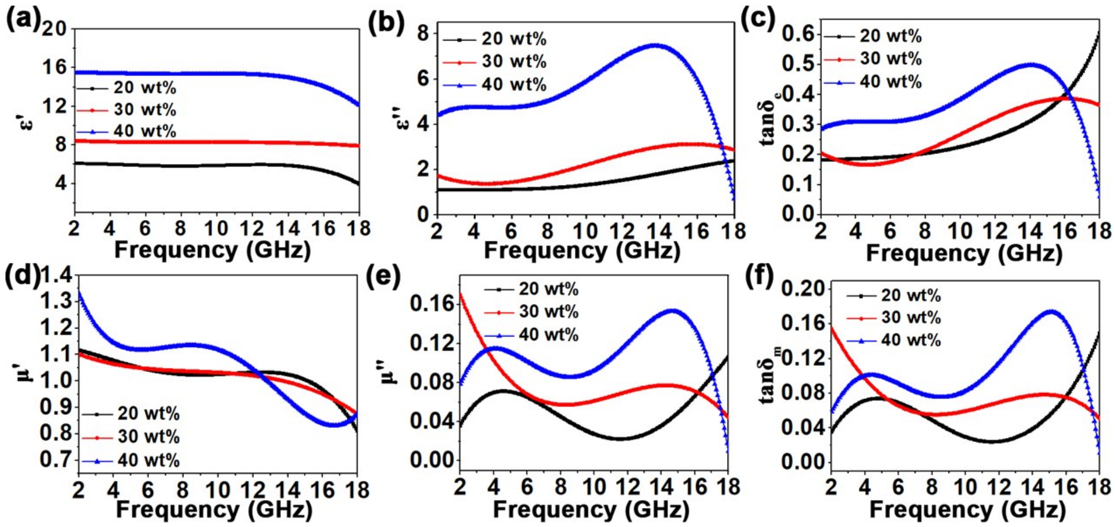

Fig. S5 Changes of the electromagnetic parameters for the flexible papers contianing as the varied $FeNi_3/Mo_2C$ contents, including the (a) ε', (b) ε'', (c) $\tan\delta_e$, (d) μ', (e) μ'' and (f) $\tan\delta_m$

Figure S6 shows the reflection loss curves of the flexible papers containing varied $FeNi_3/Mo_2C$ content. The sample containg 20 wt% $FeNi_3/Mo_2C$ exhibits relatively poor performance with the minimum RL of -18.8 dB. Increasing $FeNi_3/Mo_2C$ content to 30 wt%, better absorption with RL = -51.50 dB and EAB = 5.1 GHz at the thickness of 2.0 mm has been achieved which deteriorated with further increased $FeNi_3/Mo_2C$ content of 40 wt%.

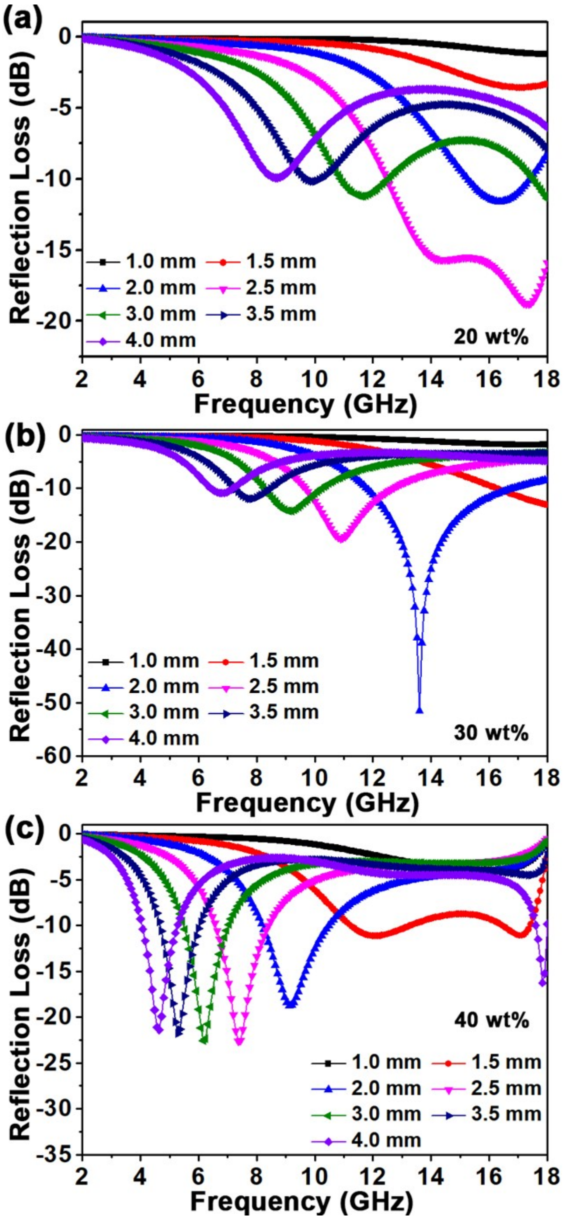

Fig. S6 Reflection loss (RL) as a function of frequency for the samples with varied $FeNi_3/Mo_2C$ content of (a) 20 wt%, (b) 30 wt% and (c) 40 wt%

Figure S7 illustrates that besides strong attenuation of the EM wave, impedance matching also needs to be considered. Although the paper containing 40 wt% $FeNi_3/Mo_2C$ exhibit the highest dielectric and magnetic loss as shown in Fig. S5c and S5f, enhanced RL is achieved for the sample with 30 wt% $FeNi_3/Mo_2C$, which can be attributed to better impedance matching.

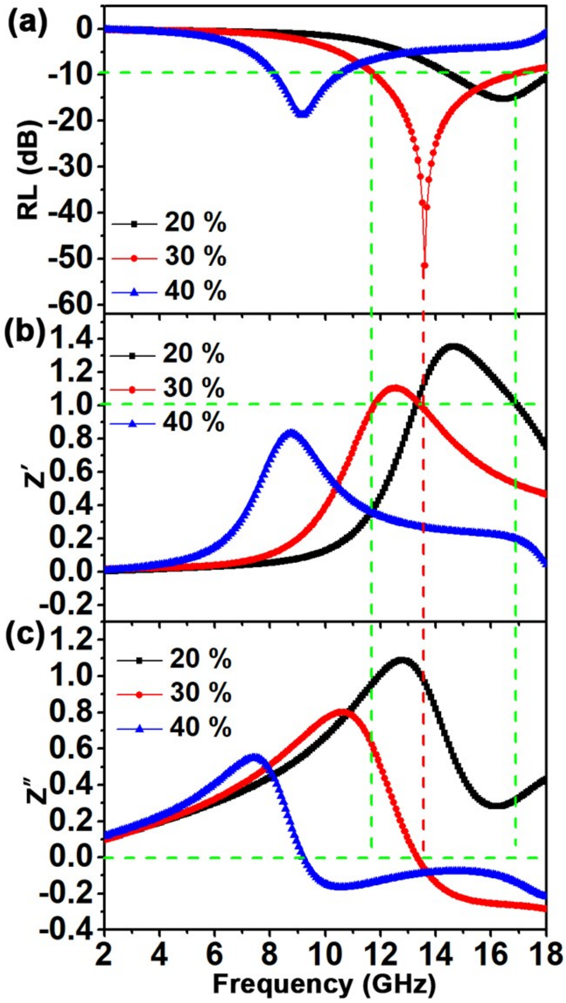

Fig.S7 Comparisons of the (a) RL, (b) real and (c) imaginary part of the impedance between the flexible papers with different content of $FeNi_3/Mo_2C$

Figure S8a-S8d show the complex permittivity and permeability of the blank flexible paper and that loaded with the $FeNi_3$ nanoparticles. Both enhanced dielectric and magnetic parameters can be achieved by the addition of the $FeNi_3$. Compared with the blank paper, the $FeNi_3$ paper exhibit slightly improved RL of 15.38 dB, EAB of 4.7 GHz at the thickness of 3.0mm(Fig. S8e and S8f). Such performance however, is much inferior to that of the $FeNi_3/Mo_2C$ papers.

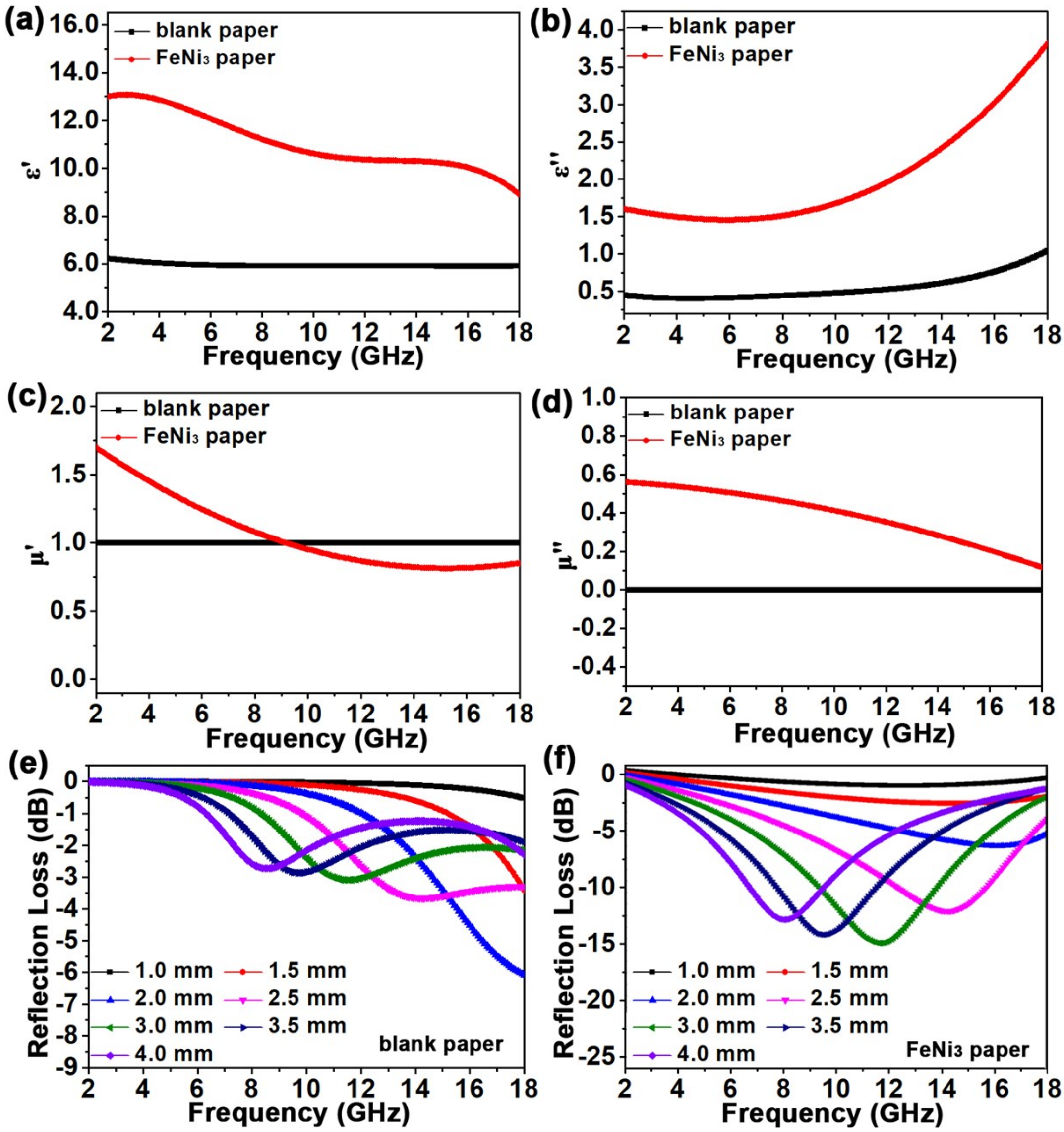

Fig. S8 (a) Real (ε') and (b) imaginary (ε'') part of the permittivity as well as (c) the real (μ') and (e) imaginary (μ'') permeability of the blank paper and that containing the $FeNi_3$. (e) & (f) Reflection loss (RL) calculated for the two samples.

Figure S9 shows the cole-cole curves of the composite absorbing papers before and after annealing. According to the Debye theory, relationship between the ε' and ε'' can be expressed by[1]:

$$\left(\varepsilon' - \frac{\varepsilon_s + \varepsilon_\infty}{2}\right)^2 + \left(\varepsilon''\right)^2 = \left(\frac{\varepsilon_s - \varepsilon_\infty}{2}\right)^2 \quad (1)$$

Where ε_s is the static dielectric constant and ε_∞ is the relative dielectric constant at high frequencies.

Consequently, the appearance of semicircles in the cole-cole curves can be correlated to Debye relaxation processes. Compared with the samples without annealing or annealed at relative low temperature (350 ℃), obvious semicircles can be observed for the composites after annealing at temperatures above 500 ℃ (Fig. S9c and S9d). Such relaxation is related to the interface polarization between Mo_2C and $FeNi_3$.

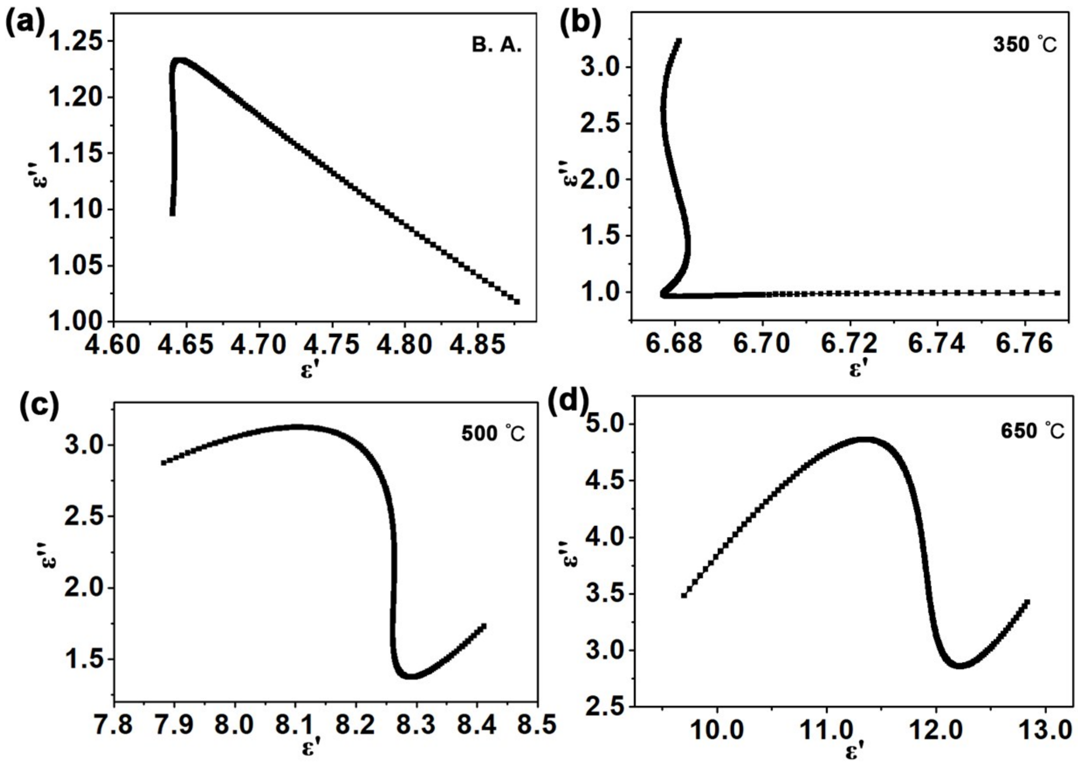

Fig. S9 Cole-cole curves of the absorbing papers containing the $FeNi_3$@Mo_2C (a) before and after annealing at (b) 350 ℃, (c) 500 ℃ and (d) 650 ℃.

Figure S10 illustrates that not only strong attenuation of the EM wave is important to achieve strong absorption, impedance matching also need to be considered. Although the attenuation factor of the flexible paper containing the $FeNi_3$@Mo_2C annealed at 650 ℃ exceed that of the sample annealed at 500 ℃ (Fig.S10b), more enhanced RL is achieved for the latter (Fig.S10a) which can be attributed to better impedance matching (Fig.S10c & S10d).

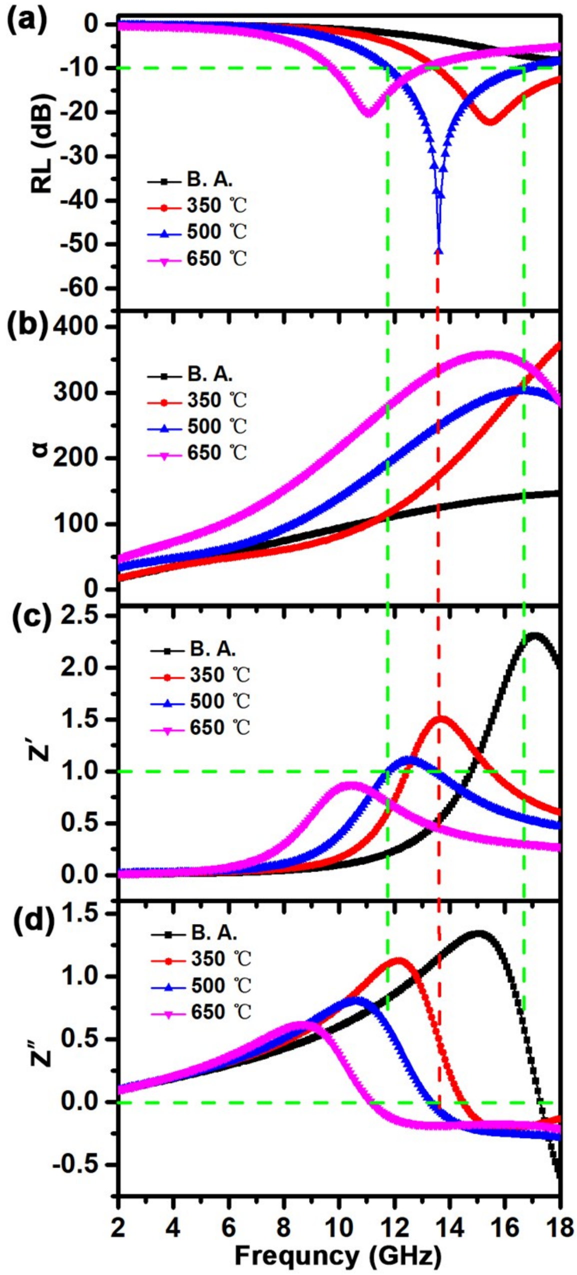

Fig.S10 Comparisons of the (a) RL, (b) attenuation coefficient α, (c) real and (d) imaginary part of the impedance between the flexible papers containing the $FeNi_3/Mo_2C$ before and after annealing at various temperatures.

Figure S11 compares the electromagnetic parameters of the absorbing paper with $FeNi_3/Mo_2C$ annealed at 500 ℃ obtained by the coaxial and waveguide methods. The ε', ε'', μ' and μ'' measured by both methods exhibit similar value and trend compared with each other.

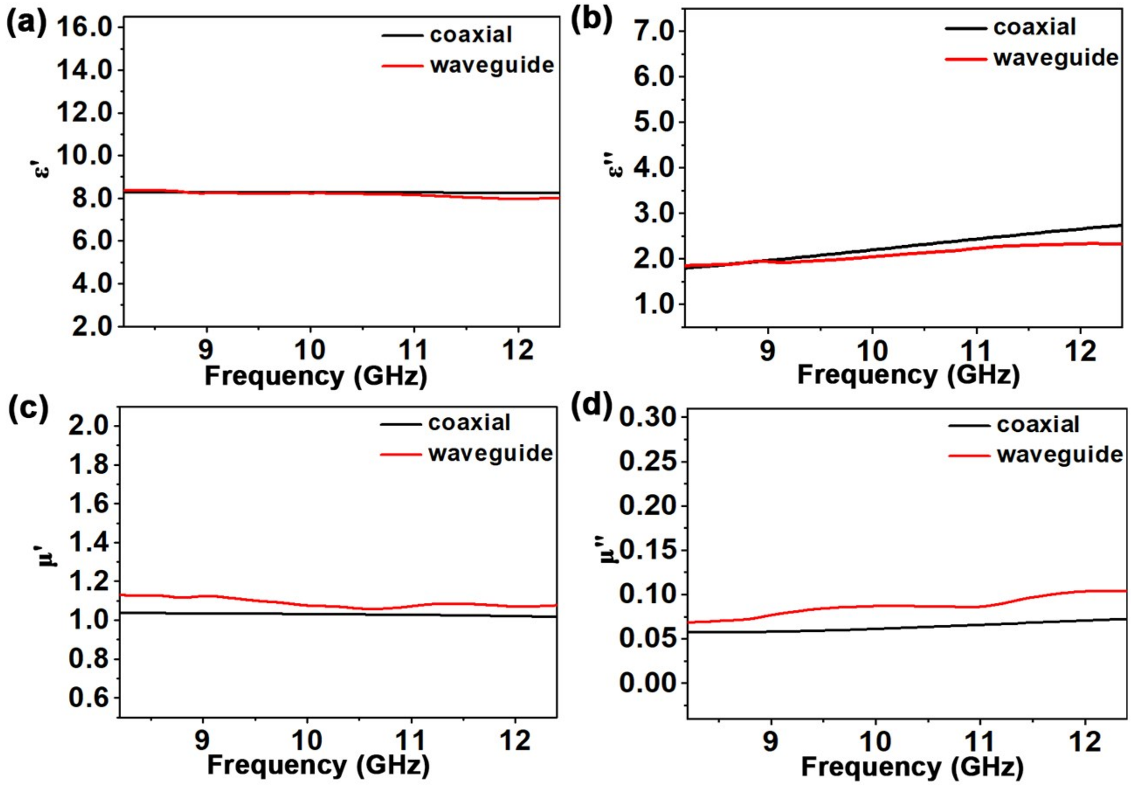

Fig.S11 The (a) ε', (b) ε'', (c) μ' and (d) μ'' measured by the coaxial and waveguide methods.

Table S1 compares the absorption performance of the $FeNi_3/Mo_2C$ paper with other related materials reported recently. The $FeNi_3/Mo_2C$ paper exhibit relatively wide EAB (5.10 GHz) and enhanced RL (-51.50 dB).

Material systems	EAB (GHz)	RL_{min}(dB)	Thickness(mm)	Filler ratio (wt%)	Ref.
Mo_2C	3.20	-49.19	2.60	20 %	2
Ni/Mo_2C-C	3.50	-55.90	2.70	15 %	3

Ni@SnO_2	4.80	-29.70	1.70	50 %	4
FeCo/graphite	1.60	-30.60	2.00	30%	5
FeCo/Al_2O_3	3.20	-30.80	2.00	—	6
FeNi/C	3.30	-32.78	1.30	40 %	7
$FeNi_3$/N-GN	3.40	-57.20	1.45	50 %	8
$FeNi_3$@C	5.08	-43.30	2.00	40 %	9
$FeNi_3$/Mo_2C	5.10	-51.50	2.00	30 %	This work

Table S1 Comparisons of the electromagnetic wave absorption performance between the $FeNi_3$/Mo_2C composites and other related materials

Reference

1. B. Zhao, B. Fan, Y. Xu, G. Shao, X. Wang, W. Zhao and R. Zhang, *ACS Appl. Mater. Interfaces*, 2015, **7,** 26217-26225.
2. S. Dai, Y. Cheng, B. Quan, X. Liang, W. Liu, Z. Yang, G. Ji and Y. Du, *Nanoscale*, 2018, **10**, 6945-6953.
3. S. Gao, J. Feng, G. Wang and B. Liang, *Front Chem.*, 2019, **7**, 427.
4. B. Zhao, X. Guo, W. Zhao, J. Deng, G. Shao, B. Fan, Z. Bai and R. Zhang, *ACS Appl. Mater. Interfaces*, 2016, **8**, 28917-28925.
5. C. Wang, R. Lv, Z. Huang, F. Kang and J. Gu, *J. Alloys Compd.*, 2011, **509**, 494-498.
6. X. Liu, D. Geng and Z. Zhang, *Appl. Phys. Lett.*, 2012, **100**, 229901.

7. C. Feng, X. Liu, Y. Sun, C. Jin and Y. Lv, *RSC Adv.*, 2014, **4**, 22710-22715.

8. J. Feng, Y. Zong, Y. Sun, Y. Zhang, X. Yang, G. Long, Y. Wang, X. H. Li and X. Zheng, *Chem. Eng. J.*, 2018, **345**, 441-451.

9. Y. Sun, X. Liu, C. Feng, J. C. Fan, Y. Lv, Y. Wang and C. Li, *J. Alloys Compd.*, 2014, **586**, 688-692.